Draft version October 16, 2020
Typeset using LaTeX **preprint** style in AASTeX62

N-body simulations of the Self–Confinement of Viscous Self–Gravitating Narrow Eccentric Planetary Ringlets

Joseph M. Hahn,[1] Douglas P. Hamilton,[2] Thomas Rimlinger,[2] and Lucy Luu[2]

[1] *Space Science Institute*
[2] *University of Maryland*

(Received not yet; Revised not yet; Accepted not yet)

Submitted to Somewhere, eventually

ABSTRACT

N-body simulations are used to illustrate how narrow eccentric planetary ringlets can evolve into a self–confining state.

Keywords: editorials, notices — miscellaneous — catalogs — surveys — update, me

1. INTRODUCTION

Narrow eccentric planetary ringlets have properties both interesting and not well understood: sharp edges, sizable eccentricity gradients, and a confinement mechanism that opposes radial spreading due to ring viscosity. Prevailing ringlet confinement mechanisms include: unseen shepherd satellites (reference), periapse pinch (ref), self gravity (ref), and self-confinement (ref). This study uses N-body simulations to show how a viscous narrow self–gravitating ringlet can evolve into a self-confining state.

2. RINGLET CONFINEMENT MECHANISMS

This section will explain the pros and cons of the various ringlet confinement mechanisms, and will then motivate the possibility that ringlets are self confining. That possibility is explored further via numerical simulations using the epi_int_lite N-body integrator.

3. EPI_INT_LITE

Epi_int_lite is a child of the epi_int N-body integrator that was used to simulate the outer edge of Saturn's B ring while it is sculpted by satellite perturbations (Hahn & Spitale 2013). The new code is very similar to its parent but differs in two significant ways: (*i.*) epi_int_lite is written in python and recoded for more efficient execution, and (*ii.*) epi_int_lite uses a more reliable drift step to handle unperturbed motion around an oblate planet (detailed in Appendix A).

Otherwise epi_int_lite's treatment of ring self–gravity and viscosity are identical to that used by the parent code; see Hahn & Spitale (2013) for additional details. The epi_int_lite source code is available

Corresponding author: Joseph M. Hahn
jhahn@spacescience.org

at https://github.com/joehahn/epi_int_lite, and the code's numerical quality is assessed in Appendix B where the output of several numerical experiments are compared against theoretical expectations.

Calculations by epi_int_lite use natural units with gravitation constant $G = 1$, central primary mass $M = 1$, and the ringlet's inner edge has initial radius $r_0 = 1$, and so the ringlet masses m_r and radii r quoted below are in units of M and r_0. Converting code output from natural units to physical units requires choosing physical values for M and r_0 and multiplying accordingly, and when this text does so it assumes Saturn's mass $M = 5.68 \times 10^{29}$ gm and a characteristic ring radius $r_0 = 1.0 \times 10^{10}$ cm. Simulation time t is in units of $T_{\rm orb}/2\pi$ where $T_{\rm orb} = 2\pi\sqrt{r_0^3/GM}$ is the orbit period at r_0, so divide simulation time t by 2π and then multiply by $T_{\rm orb}$ to convert simulation time from natural to physical units. The simulated particles' motions during the drift step are also sensitive to the J_2 portion of the primary's non-spherical gravity component (see Appendix B), and all simulations adopt Saturn-like values of $J_2 = 0.01$ and $R_p = r_0/2$ where R_p is the planet's mean radius.

Initially all particles are assigned to various streamlines across the simulated ringlet. A streamline is a closed eccentric path around the primary, and the N_p particles in a given streamline are initially assigned a common semimajor axis a and eccentricity e and are distributed uniformly in longitude. Most of the simulations described below employ only $N_s = 2$ streamlines, so that the model output can be benchmarked against theoretical treatments that also treat the ringlet as two gravitating rings (e.g. Borderies et al. 1983). But the following also performs a few higher-resolution simulations using $N_s = 11$ streamlines, to demonstrate that the $N_s = 2$ treatment is perfectly adequate and reproduces all the relevant dynamics. All simulations use $N_p = 241$ particles per streamline, and the total number of particles is $N_s N_p$. Note that the assignment of particles to a given streamline is merely for labeling purposes, as particles are still free to wander in response to the ring's internal forces, namely, ring gravity and viscosity. But as Hahn & Spitale (2013) as well as this work shows, the simulated ring stays coherent and highly organized throughout the simulation such that particles on the same streamline do not pass each other longitudinally, nor do they cross adjacent streamlines. Because the simulated ringlet stays highly organized, there is no radial or longitudinal mixing of the ring particles, and simulated particles preserve their streamline membership over time.

4. N-BODY SIMULATIONS OF VISCOUS GRAVITATING RINGLETS

This Section describes a suite of N-body simulations of narrow viscous gravitating planetary ringlets, to highlight the range of initial ringlet conditions the do evolve into a self-confining state, and those that do not.

4.1. *nominal model*

Figure 1 shows the semimajor axis evolution of what is referred to as the nominal model since this ringlet readily evolves into a self-confining state. The simulated ringlet is composed of $N_s = 2$ streamlines having $N_p = 241$ particles per streamline, and the integrator timestep is $\Delta t = 0.5$ in natural units, so the integrator samples the particles' orbits $2\pi/\Delta t \simeq 13$ times per orbit, and this ringlet is evolved for 4.7×10^3 orbits, which requires 15 minutes execution time on a 5 year old laptop. The ringlet's mass is $m_r = 5 \times 10^{-10}$, its shear viscosity is $\nu_s = 2.5 \times 10^{-12}$, and its bulk viscosity is $\nu_b = \nu_s$. The ringet's initial radial width is $\Delta a_0 = 3 \times 10^{-4}$, its initial eccentricity is $e = 0.01$, and its eccentricity gradient is initially zero. A convenient measure of time is the ringlet's viscous radial spreading timescale

$$\tau_\nu = \frac{\Delta a_0^2}{12\nu_s}, \tag{1}$$

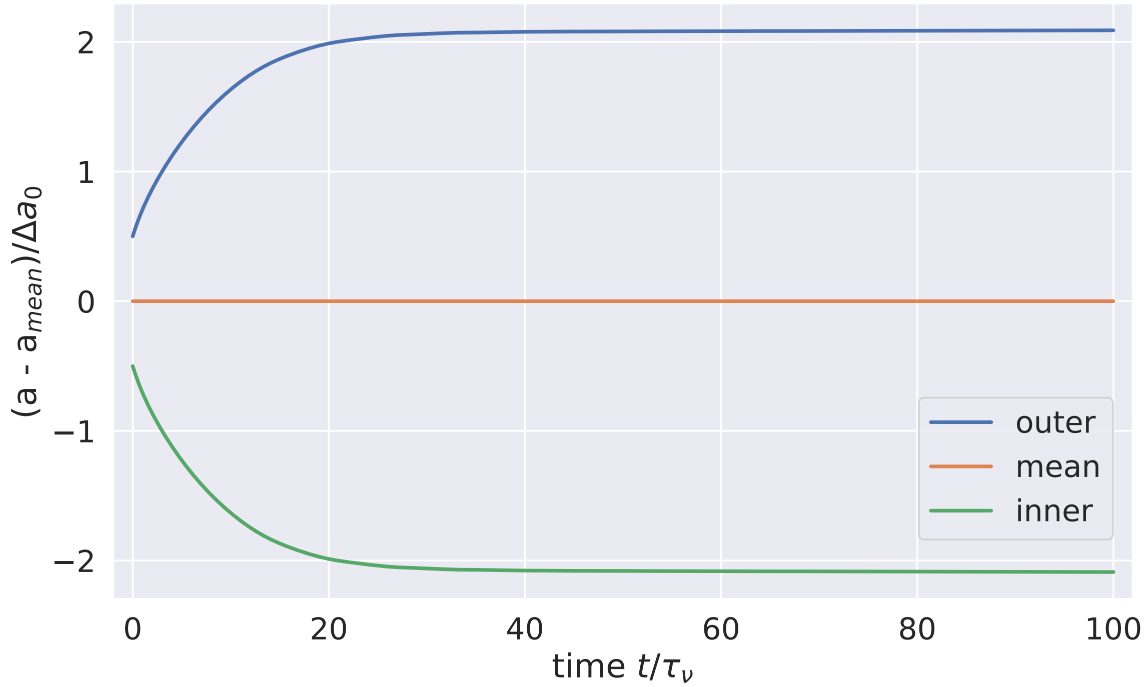

Figure 1. Evolution of the nominal ringlet's semimajor axes a versus time t in units of the ringlet's viscous time τ_ν. This ringlet is composed of $N_s = 2$ streamlines, and the outer (blue) and inner (green) streamlines' semimajor axes are plotted relative to their mean $a_{\rm mean}$, and displayed in units of the ringlet's initial width $\Delta a_0 = 3\times10^{-4}$ in natural units (*i.e.* $G = M = r_0 = 1$). The simulated ringlet has total mass $m_r = 5\times10^{-10}$, shear viscosity $\nu_s = 2.5\times10^{-12}$, and initial eccentricity $e = 0.01$, and see Section 4.1 to convert m_r, a and ν_s from natural units to physical units.

which can be inferred from Eqn. (2.13) of Pringle (1981). This simulation's viscous timescale is $\tau_\nu = 3.0\times10^3$ in natural units or $\tau_\nu/2\pi = 4.8\times10^2$ orbital periods. If this ringlet were orbiting Saturn at $r_0 = 1.0\times10^{10}$ cm then the simulated ringlet's physical mass would be $m_r = 2.8\times10^{20}$ gm which is equivalent to the mass of a 41 km radius iceball assuming a volume density $\rho = 1$ gm/cm^3, and the ringlet's initial radial width would be $\Delta a_0 = 3\times10^{-4}r_0 = 30$ km. This ringlet's orbit period would be $T_{orb} = 2\pi\sqrt{r_0^3/GM} = 9.0$ hours in physical units, so the ringlet's viscous timescale is $\tau_\nu = 12$ years, and so its shear viscosity is $\nu_s = \Delta a_0^2/12\tau_\nu = 4.8\times10^4$ cm^2/sec when evaluated in physical units. This ringlet's initial surface density would be $\sigma = m_r/2\pi r_0\Delta a_0 = 1500$ gm/cm^2, but Figs. 1–2 show that shrinks by a factor of 4 as the ringlet's sememajor axis width Δa grows via viscous spreading until it settles into the self-confining state at time $t\sim20\tau_\nu$. This so-called nominal ringlet is probably overdense and overly viscous compared to known planetary ringlets, but that is by design so that the simulated ringlet quickly settles into the self-confining state. Section XX also shows how outcomes scale when a wide variety of alternate initial masses, orbits, and viscosities are also considered.

Figure 3 shows that the outer streamline's eccentricity initially grows at the expense of the inner streamline's, and this is a consequence the self-gravitating ringlet's secular perturbations of itself, which is also demonstrated in Appendix C. Figure 4 shows the ringlet's eccentricity difference $\Delta e = e_{\rm outer} - e_{\rm inner}$ and longitude of periapse difference $\Delta\tilde{\omega} = \tilde{\omega}_{\rm outer} - \tilde{\omega}_{\rm inner}$, which both settle into equilibrium values after the ringlet arrives in the self-confining state.

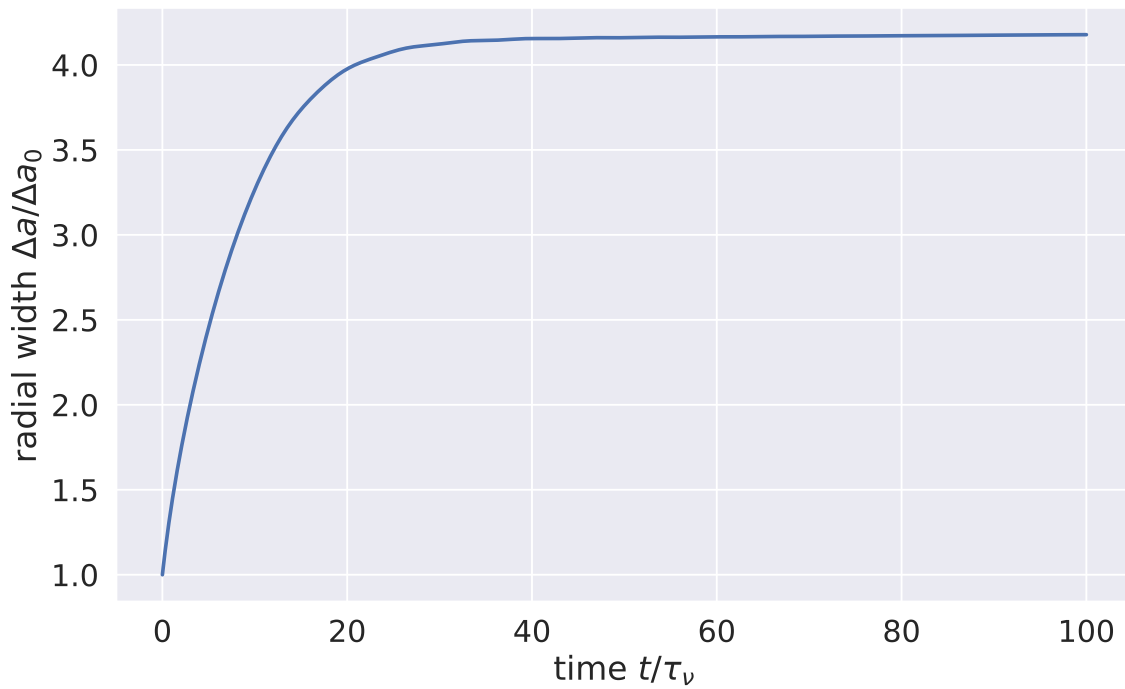

Figure 2. The nominal ringlet's semimajor axis width $\Delta a = a_{\rm outer} - a_{\rm inner}$ over time, in units of its initial radial width Δa_0.

It is convenient to recast these orbit element differences as dimensionless gradients

$$e' = a\frac{de}{da} \qquad \text{and} \qquad \tilde{\omega}' = ea\frac{d\tilde{\omega}}{da} \tag{2}$$

as these are the terms that contribute to the nonlinearity parameter of Borderies et al. (1983):

$$q = \sqrt{e'^2 + \tilde{\omega}'^2}. \tag{3}$$

See also Fig. 5 which plot's the nominal ringlet's dimensionless eccentricity gradient e', dimensionless periapse twist $\tilde{\omega}'$, and nonlinearity parameter q versus time. All simulations examined here have $|\tilde{\omega}'| \ll |e'|$ so that $q \simeq |e'|$, and all simulated self-confining ringlets have a positive eccenticity gradient and a negative periapse twist such that the outer ringlet's periapse trails the inner ringlet's, consistent with the findings of Borderies et al. (1983).

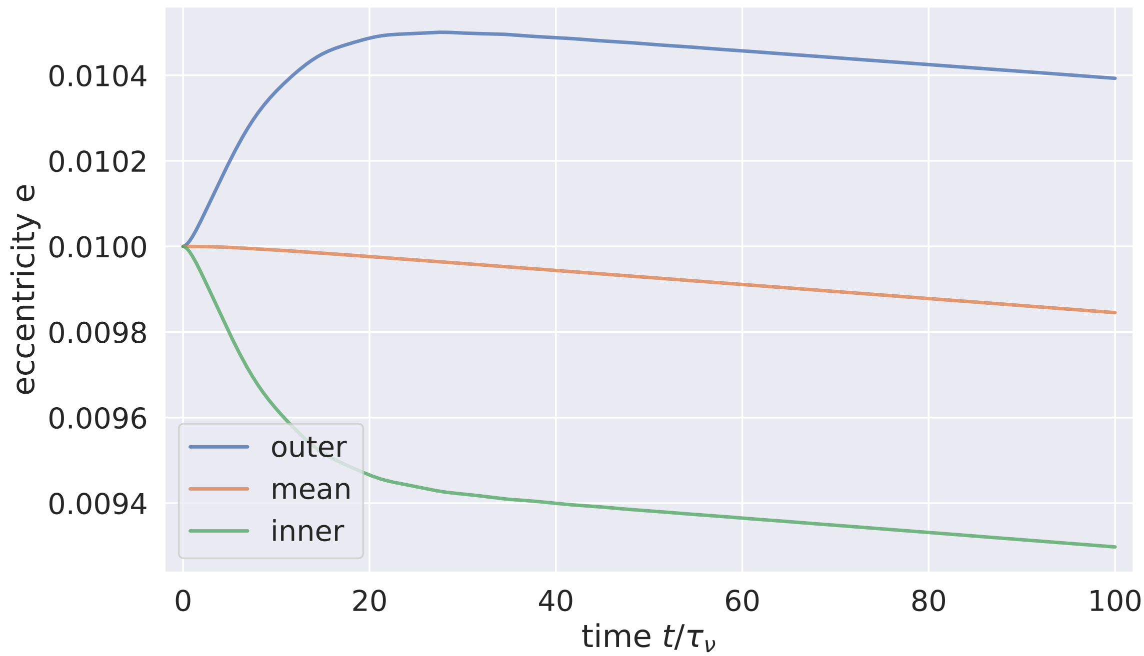

Figure 3. The nominal ringlet's eccentricity evolution.

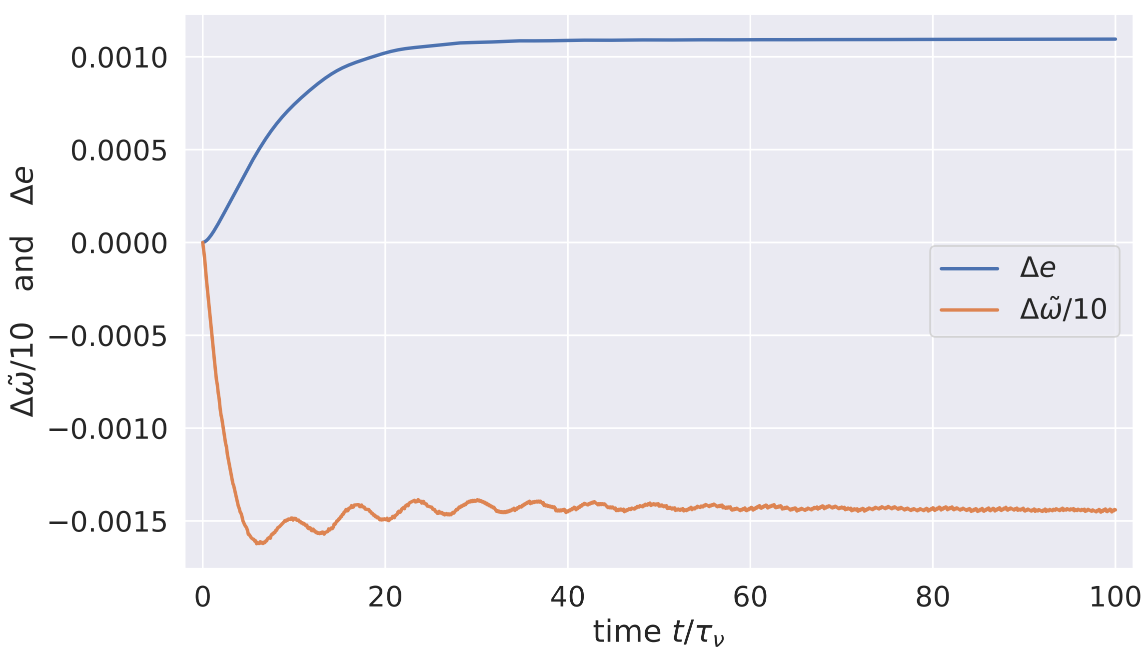

Figure 4. The nominal ringlet's eccentricity difference $\Delta e = e_{\rm outer} - e_{\rm inner}$ and longitude of periapse difference $\Delta\tilde{\omega} = \tilde{\omega}_{\rm outer} - \tilde{\omega}_{\rm inner}$ divided by 10.

4.2. *viscous angular momentum transport*

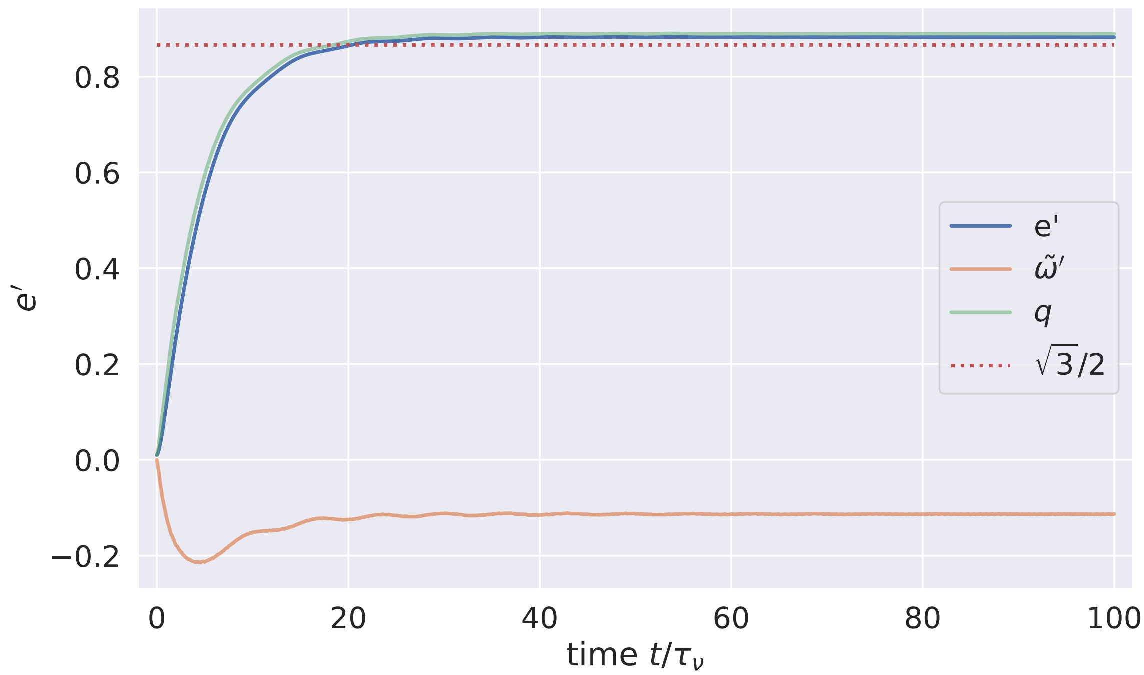

Figure 5. The nominal ringlet's dimensionless eccentricity gradient $e' = a\Delta e/\Delta a$ (blue curve), dimensionless periapse twist $\tilde{\omega}' = ea\Delta\tilde{\omega}/\Delta a$ (orange), and nonlinearity parameter $q = \sqrt{e'^2 + \tilde{\omega}'^2}$ (green) versus time t/τ_ν. Dotted red line is the threshold for self-confinement in a non-gravitating ringlet, $e' = \sqrt{3}/2 \simeq 0.866$

The ringlet's evolution is readily understood when the ringlet's viscous flux of angular momentum is considered; that flux is

$$F_\nu(r, \theta) = -\nu_s \sigma r^2 \frac{\partial \omega}{\partial r} \tag{4}$$

(Hahn & Spitale 2013) when written as a function of spatial coordinates and angular velocity $\omega = \dot{\theta}$ (Eqn. XX). If we consider a small arc of ring material of transverse length $d\ell$, then $F_\nu d\ell$ would be the torque that arc exert exerts on ring matter just exterior, due to viscous friction, so that is the rate that friction transmits angular momentum radially across that arc. And when F_ν is evaluated along a single eccentric streamline of semimajor axis a, the above simplifies to

$$F_\nu(a, \varphi) = F_{\nu,0} \frac{1 - \frac{4}{3}e' \cos\varphi}{(1 - e' \cos\varphi)^2} \tag{5}$$

where $\varphi = \theta - \tilde{\omega}$ is the longitude relative to periapse (see Borderies et al. 1982 and Appendix D) and $F_{\nu,0} = \frac{3}{2}\nu_s \sigma_0 a \Omega$ is the viscous angular momentum flux through a circular streamline of semimajor axis a and angular speed $\Omega(a)$ and assuming $|\tilde{\omega}'| \ll e'$ so that $q \simeq e'$. Integrating the above around the streamline's circumference then yields its angular momentum luminosity,

$$L_\nu(a) = \oint F_\nu(e', \varphi) r d\varphi = L_{\nu,0} \frac{1 - \frac{4}{3}e'^2}{(1 - e'^2)^{3/2}}, \tag{6}$$

which is the torque that one streamline exerts on its exterior neighbor due to viscous friction (Borderies et al. 1982 and Appendix D), where $L_{\nu,0} = 3\pi\nu_s \sigma_0 a^2 \Omega$ viscous angular momentum luminosity of a circular streamline.

Borderies et al. (1982) examine angular momentum transport through a viscous eccentric but non-gravitating ringlet, and use Eqns. (5–6) to show that this transport has three regimes distinguished by the ringlet's e':

1. $e' < 3/4$, so the ringlet's viscous angular momentum flux $F_\nu(\varphi) > 0$ at all ringlet longitudes θ. The ringlet's viscous angular momentum luminosity $L_\nu > 0$, so viscous friction transports angular momentum radially outwards, so inner ring matter evolves to smaller orbits while exterior ring matter evolves outwards, and the ringlet spreads radially.

2. $3/4 \leq e' < \sqrt{3}/4$. In this regime there is a range of longitudes θ where the viscous angular momentum flux is reversed such that $F_\nu(\varphi) < 0$. Nonetheless L_ν, which is the orbit-average of $F_\nu(\varphi)$, is positive and the ringlet still spreads radially, albeit slower than when $e' < 0.75$.

3. $e' \geq \sqrt{3}/4$. Viscous angular momentum flux reversal is complete such that $L_\nu < 0$, viscous friction transports angular momentum radially inwards, and the ringlet shrinks radially. But if $e' = \sqrt{3}/4 \simeq 0.866$ then $L_\nu = 0$ and the ringlet's radial evolution ceases, and the viscous but non-gravitating ringlet is self confining.

Note though that the nominal ringlet's eccentricity gradient exceeds the $e' = \sqrt{3}/4 \simeq 0.866$ threshold (which is the dotted red line in Fig. 5) when it settles into self-confinement. This is due to the ringlet's self-gravity, which also transports angular momentum radially through the ringlet.

Figure 6 shows the nominal ringlet's viscous angular momentum flux F_ν versus relative longitude $\varphi = \theta - \tilde{\omega}$ at selected times t. Early in the ringlet's evolution when time $t \leq 8\tau_\nu$ (blue, orange, green, red, and purple curves), the ringlet is in regime 1 since $e' < 0.75$ and $F_\nu(\varphi) > 0$ at all longitudes. But by time $t = 10\tau_\nu$ (brown curve), this ringlet's eccentricity gradient exceeds 0.75, and angular momentum flux reversal $F_\nu(\varphi) < 0$ occurs near periapse where $|\varphi| \simeq 0$ where the ringlet is most overdense due to its eccentricity gradient, see also Fig. 7; this ringlet is in regime 2 and its radial spreading is reduced by angular momentum flux reversal. And by time $t = 20\tau_\nu$ (brown curve), this ringlet is seemingly in regime 3 since $e' = 0.866$, so one might expect the ringlet's spreading to have stalled by now, but keep in mind that the above analysis ignores any transport of angular momentum via ringlet self–gravity. Figure 2 shows that this gravitating ringlet's spreading has ceased soon after time $t \simeq 35\tau_\nu$, at which point $e' = 0.88$ (cyan curve), angular momentum flux reversal is nearly complete, with the ringlet's total angular momentum luminosity $L = L_\nu + L_g = 0$ is very close to zero. Figure 8 and Fig. 9 show that the ringlet's positive viscous angular momentum luminosity L_ν is nearly matched by the by the ringlet's negative gravitational angular momentum luminosity L_g. *But I still need to explain why L isn't precisely zero when ringlet is seemingly self–confining...*

Figure 10 shows how viscosity and self-gravity transport angular momentum across a self-confining ringlet at various longitudes φ. That figure shows that ringlet viscosity transports angular momentum inwards *i.e.* $F_\nu(\varphi) < 0$ near periapse, and outwards with $F_\nu(\varphi) > 0$ at all other longitudes. Which is rather distinct from the ringlet's gravitational transport, which has $F_g(\varphi) < 0$ as ring-matter travels towards periapse, and outwards $F_g(\varphi) > 0$ after periapse. Despite these spatial differences, the influence of both forces still sum to zero in the orbit-integrated sense *i.e.* $\oint (F_\nu + F_g) r d\varphi = 0$ after the ringlet has settled into the self-confining state.

Ring viscosity and self-gravity can also transport energy across the ring, and that is assessed in Appendix E.

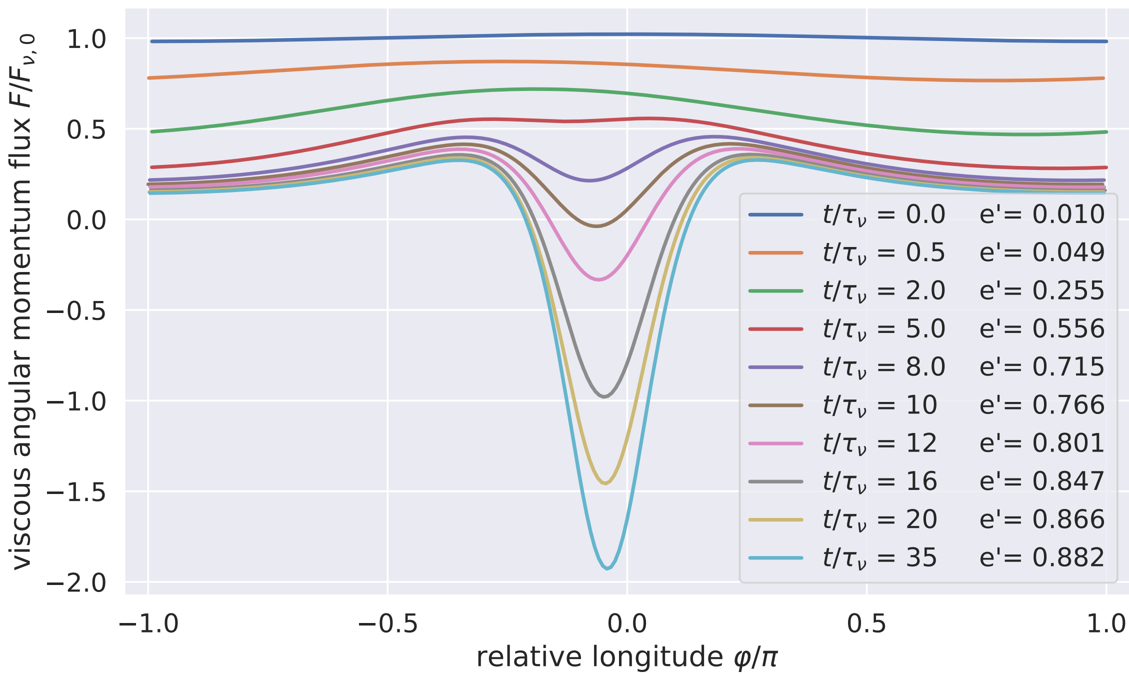

Figure 6. The nominal ringlet's viscous angular momentum flux $F_\nu(\varphi)$, Eqn. (5), is plotted versus ringlet relative longitude $\varphi = \theta - \tilde{\omega}$ about the ringlet's inner streamline at selected times t/τ_ν, with the ringlet's eccentricy gradient e' also indicated.

This research was supported by the National Science Foundation via Grant No. AST-1313013.

APPENDIX

A. APPENDIX A

Derive the more accurate drift step used by epi_int_lite...

B. APPENDIX B

Compare epi_int_lite to theoretical predictions

C. APPENDIX D

This examines the viscous evolution of a narrow eccentric non-gravitating ringlet that is identical to the nominal ringlet of Section 4.1 but with ringlet self-gravity neglected and $J_2 = 0$. As the orange curve in Fig. 11 shows, the non-gravitating ringlet's radial width Δa grows steadily over time due to ringlet viscosity, long after the nominal self-gravitating ringlet (blue curve) has settled into the self-confining state by time $t \sim 15\tau_\nu$. This is due to the ringlet's secular gravitational perturbations of itself, which tends to excites the ringlet's outer streamline's eccentricity at the expense of the inner streamline (see Fig. 3) until the ringlet eccentricity gradient e' (blue curve in Fig. 12) grows beyond the limit required for complete angular momentum flux reversal that results in the ringlet's radial confinement (dotted line). Note that viscosity also excites the non-gravitating ringlet's eccentricity gradient some (orange curve), but not sufficiently to halt the ringlet's viscous spreading.

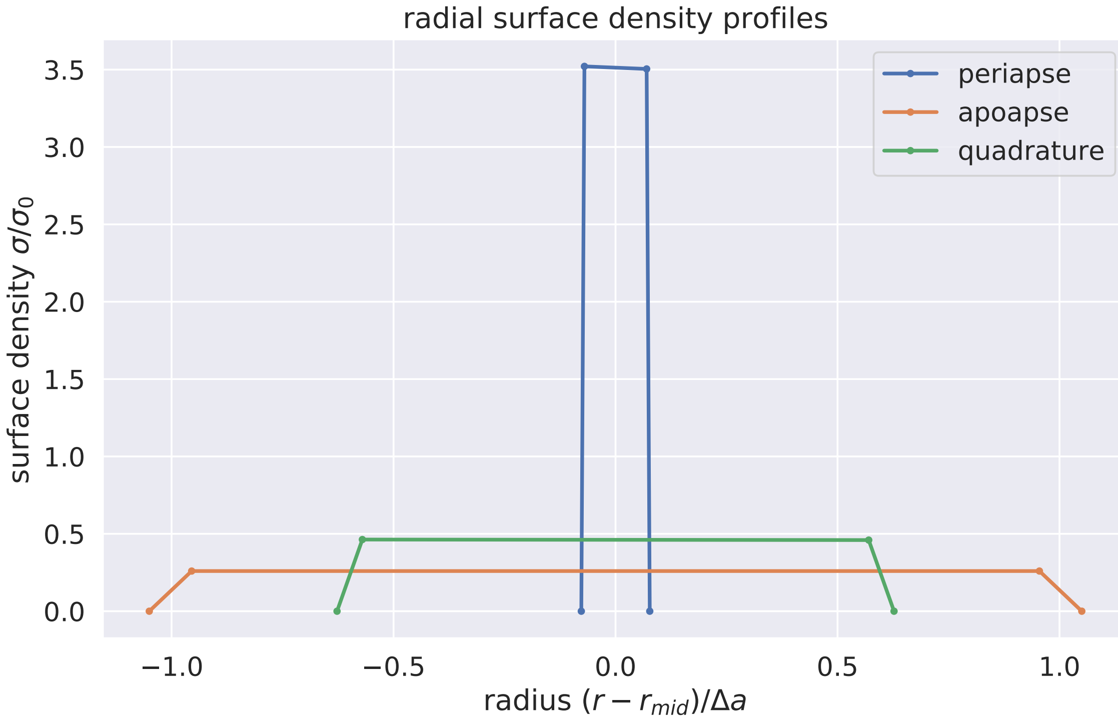

Figure 7. Radial profiles of the nominal ringlet's surface density $\sigma(\varphi)$ at time $t/\tau_\nu = 100$ when the ringlet is self-confining. Each surface density profile is plotted versus radial distance r relative to r_{mid}, which is the ringlet's midpoint along relative longitude $\varphi = \theta - \tilde{\omega}$, with those radial distances $r - r_{mid}$ measured in units of the ringlet's final semimajor axis width Δa, and surface density is shown in units of the ringlet's longitudinally-averaged surface density σ_0. Radial surface density profiles are plotted along the ringlet's periapse ($\varphi = 0$, blue curve), which is where the ringlet's streamlines are most concentrated and surface denisity σ is greatest due to the ringlet's eccentricity gradient e', at quadrature ($|\varphi| = \pi/2$, green curve), and at apoapse ($|\varphi| = \pi$, orange curve) where streamlines have their greatest separation and ringlet surface density is lowest. This ringlet's surface density contrast, between periapse and apoapse, is 14.

D. APPENDIX E

This Appendix will use the orbit elements derived in Appendix A to derive Eqn. 5 from 4, and then Eqn. (6).

E. APPENDIX F

Viscous and gravitational energy transport...

REFERENCES

Borderies, N., Goldreich, P., & Tremaine, S. 1982, Nature, 299, 209

—. 1983, Icarus, 55, 124

Hahn, J. M., & Spitale, J. N. 2013, ApJ, 772, 122

Pringle, J. E. 1981, ARA&A, 19, 137

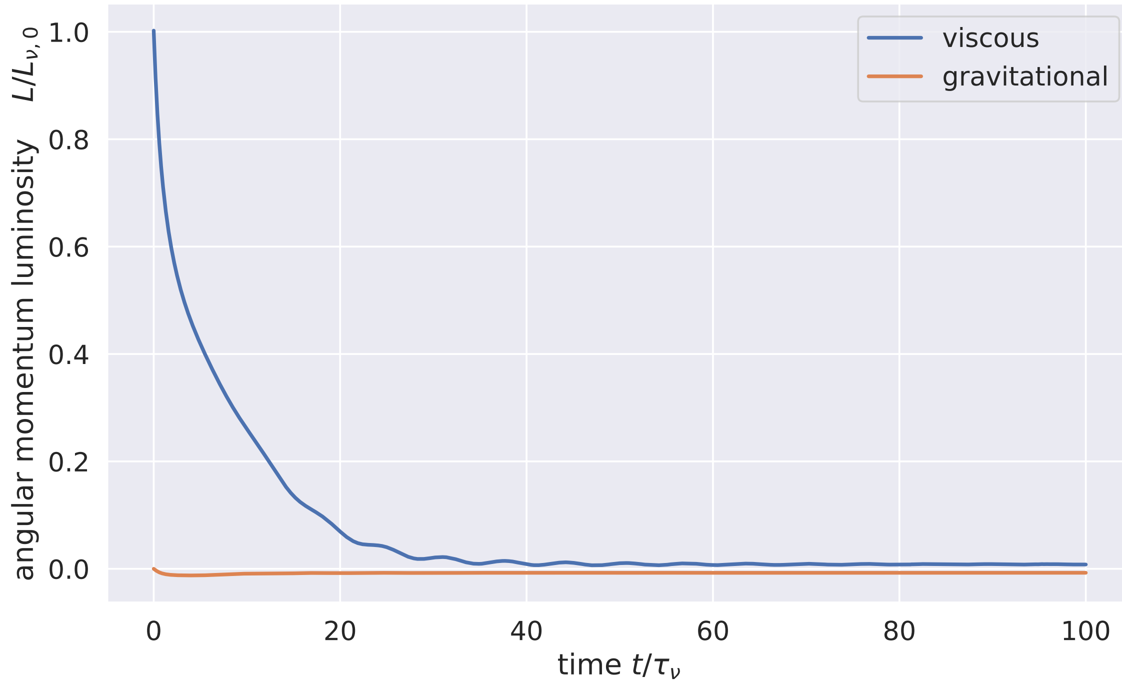

Figure 8. Nominal ringlet's viscous angular momentum luminosity $L_\nu/L_{\nu,0}$ (blue curve) versus time t/τ_ν, where $L_{\nu,0}$ is circular ring's viscous angular momentum luminosity, as well as the ringlet gravitational angular momentum luminosity L_g (orange curve) in units of $L_{\nu,0}$.

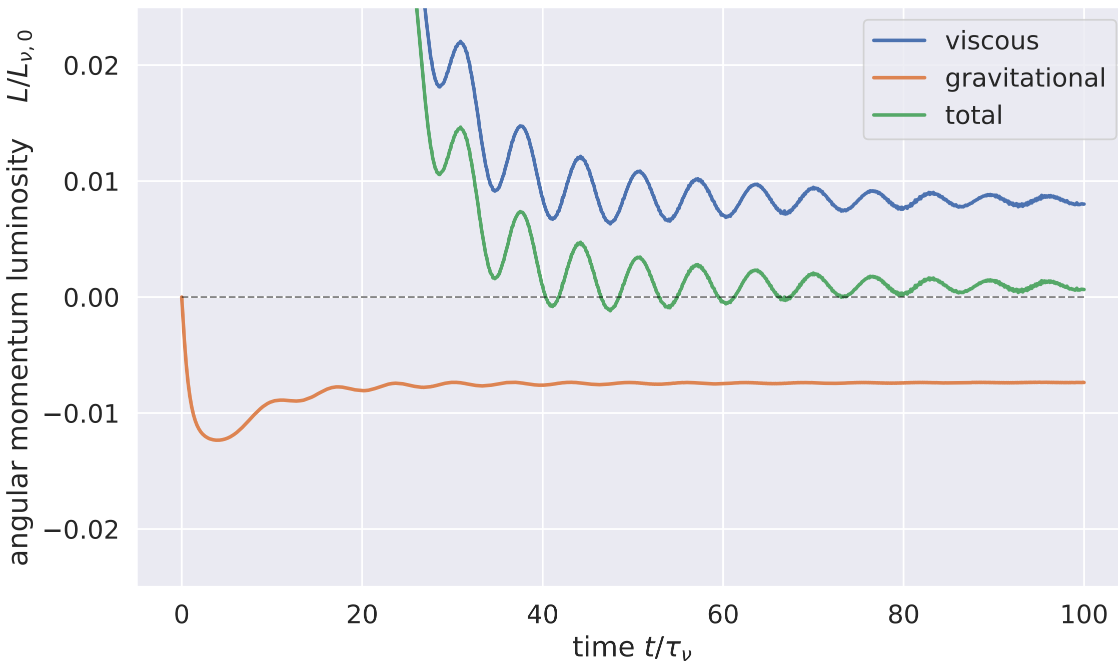

Figure 9. Figure 8 is replotted to highlight that the ringlet's viscous angular momentum luminosity L_ν (blue curve) always stays positive (indicating that the viscous transport of angular momentum is radially outwards) which is nearly balanced by the ringlet's negative (*i.e.* inwards) gravitational angular momentum luminosity L_g (orange) after time $t \gg 35\tau_\nu$.

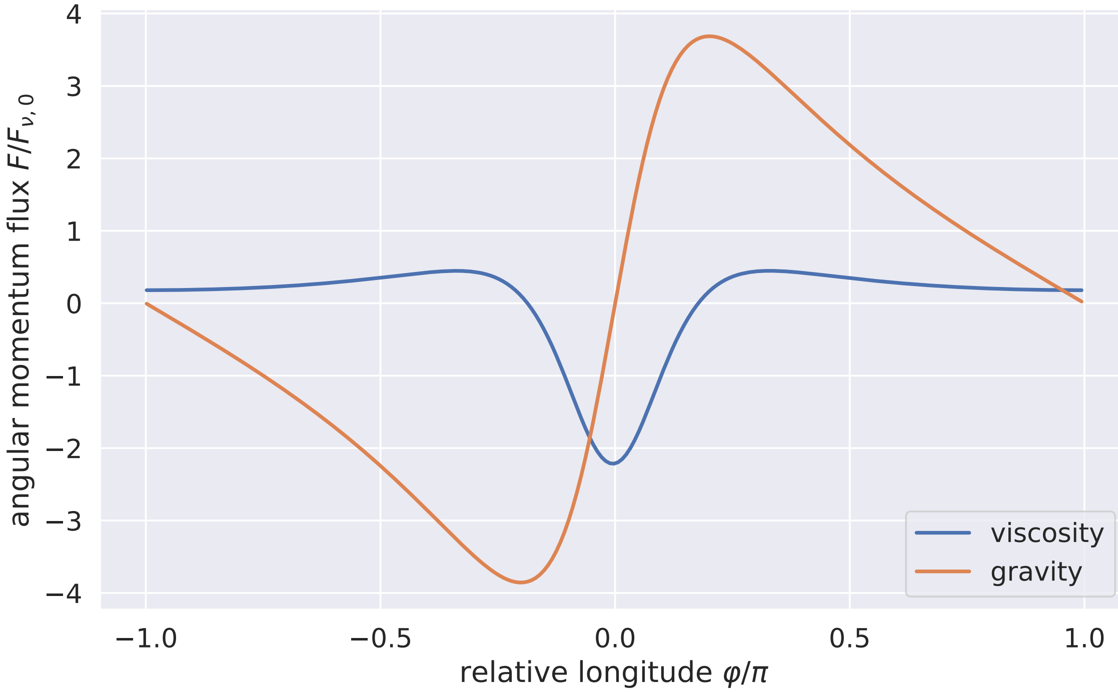

Figure 10. The nominal ringlet's viscous angular momentum flux $F_\nu(\varphi)$ (blue curve), plotted in units of $F_{\nu,0}$ and versus relative longitude φ at time $t = 50\tau_\nu$, as well as the ringlet's gravitational angular momentum flux $F_g(\varphi)$ (orange curve).

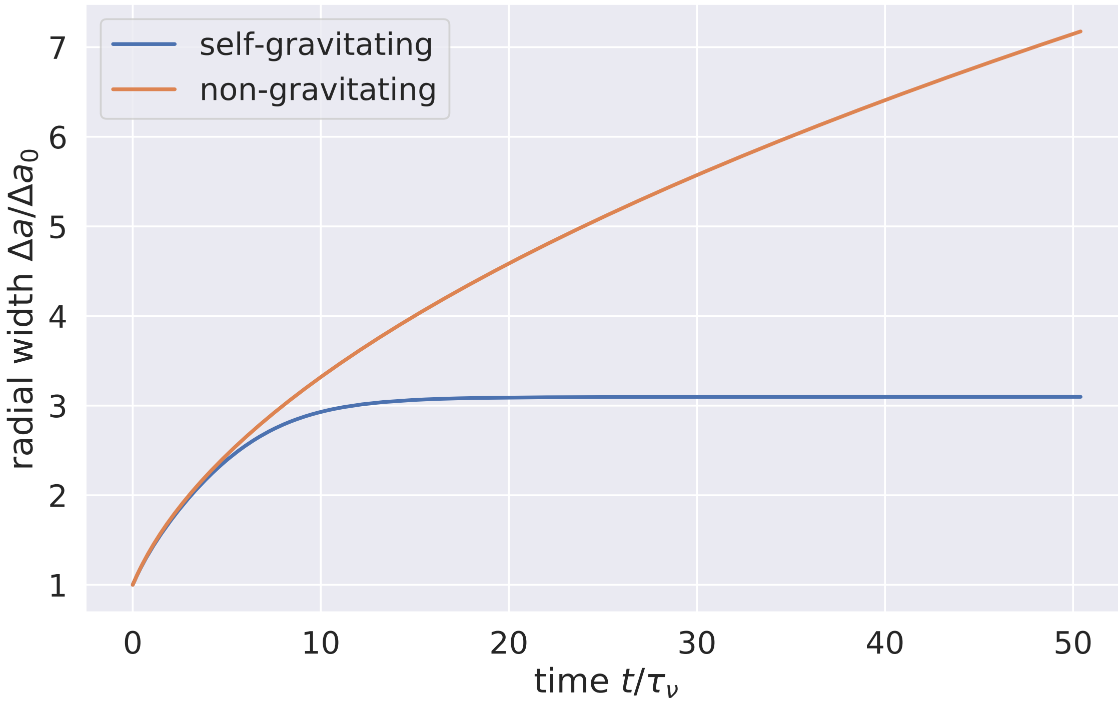

Figure 11. Blue curve is the nominal ringlet's semimajor axis width Δa versus time t, and this ringlet's radial spreading ceases by time $t \sim 15\tau_\nu$ when it's self-gravity has excited the ringlet's eccentricity gradient e' sufficiently; see blue curve in Fig. 12. Orange curve shows that the non-gravitating ringlet's Δa grows without limit due to the ringlet's much lower eccentricity gradient. Note that planetary oblateness would cause the non-gravitating streamlines to precess differentially and eventually cross when $J_s > 0$, so the non-gravitating simulation also sets $J_2 = 0$ to avoid differential precession.

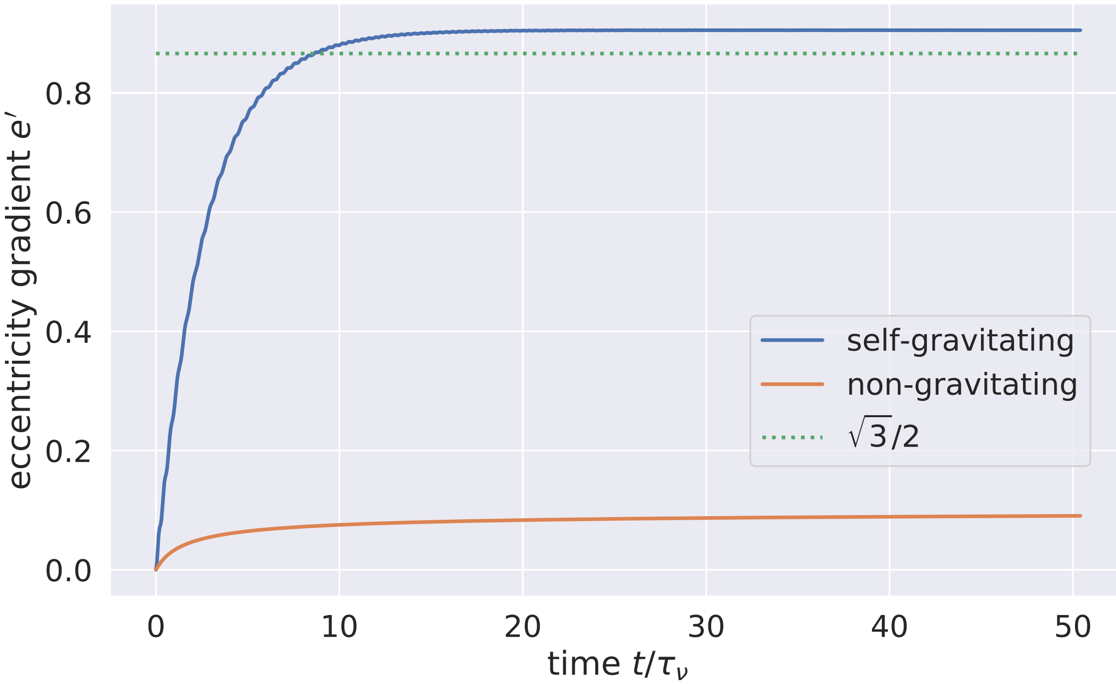

Figure 12. blah